Eur. Phys. J. B **9**, 29–36 (1999)

THE EUROPEAN PHYSICAL JOURNAL B

EDP Sciences

Self-consistent electronic structure of quantum wells by invariant embedding method

Q. Guo, Y.P. Feng, H.C. Poon, and C.K. Ong[a]

Department of Physics, National University of Singapore, Singapore 119260

Received 21 September

Abstract. A new approach based on the invariant embedding method for the self-consistent calculation of electronic structure of quantum wells is presented and is applied to both neutral quantum well and parabolic quantum well. Numerical results obtained for these structures agree very well with those of previous theoretical and experiment studies. The present approach is expected to lead to a more efficient and stable scheme for the calculation of electronic band structure of quantum structures. Realistic boundary conditions are naturally taken into account in the present calculation which provides a convenient way for studying boundary effects.

PACS. 71.10.-w Theories and models of many electron systems – 73.20.Dx Electron states in low-dimensional structures (superlattices, quantum well structures and multilayers)

1 Introduction

The electronic structure of a jellium surface was first treated self-consistently in the local density approximation (LDA) by Lang and Kohn [1]. It was later extended to the study of electronic structures of neutral and parabolic quantum wells [2–4]. Most of these works on the self-consistent calculation of electronic structures in quantum wells were based on direct solution of the Schrödinger equation, in which eigenfunctions are obtained by numerically integrating the Schrödinger equation and eigenvalues are usually found by binary searching over an energy range. The electron density is then calculated from the eigenfunctions and eigenvalues.

In the present work, we present an alternative approach for the self-consistent calculation of the electronic structure of quantum wells. The method is based on the Green's function approach in the complex energy plane. It is well known that the electron distribution around an impurity atom is related to its scattering phase shifts [5], from which the Friedel's sum rule is derived. It can be similarly proved that the Green's function at a certain plane parallel to the epitaxial layers of the quantum well can be written in terms of the reflection matrices from both sides of the plane. In this approach, we first calculate the Green's function based on the invariant embedding method. The electron density is obtained simply by integrating the Green's function over a contour in the complex energy plane, the electron density can thus be obtained without the calculation of eigenvalues and eigenfunctions in the self-consistent loop.

It is known that a small error in the electron density can induce a relatively large error in the potential. For the continuum of excited states of quantum wells or the quasi-continuum of valence states of wide quantum wells and superlattices, binary searching for energy values is usually inefficient. In contrast, in the present Green's function approach, the electron density is calculated by integrating the Green's function over a contour in the complex energy plane. Thus numerical errors in eigenfunctions and eigenvalues will not affect the accuracy of the electron density. As the integrand is smooth, only a few integration points are required. Therefore, the method provides a more efficient and stable scheme for the self-consistent calculation of electronic structures of quantum wells.

Even though it has been shown that the boundary conditions artificially imposed in the self-consistent calculation of electronic structure influence significantly the excitation spectra in neutral quantum wells (NQW) [4,6,7], such effects have not been fully investigated due to limitations of the solution-following method. The boundary conditions involved in our approach mimics the physical condition in a neutral quantum well and represents a more realistic approximation to the parabolic quantum well, compared to the "hard wall" boundary conditions used in previous calculations. Furthermore, the boundary condition is embedded in the calculation of the Green's function, boundary effects in quantum well structures can be conveniently studied using the present approach.

The invariant embedding method has previously been applied to the study of electronic structure of jellium surface [8], atom-molecule scattering [9] and reflection high energy electron diffraction (RHEED) [10]. Especially in three dimensional cases, the invariant embedding method

[a] e-mail: phyock@leonis.nus.edu.sg

is known to lead to numerically more stable schemes than the solution-following method.

2 Theory

For a typical $Ga_{1-x}Al_xAs$ quantum well, the electron effective mass, m^*, is about 0.067 m_0, where m_0 is the free electron mass, and the dielectric constant is around 13.0. The effective Bohr radius, a_0, in such a material is thus approximately 100 Å. Since the effective Bohr radius is much larger than the lattice constant, the envelope function approximation [11] can be adopted in the calculation of electronic structure in such a system. We can therefore ignore the crystalline structure of the host and treat the conduction band edge, E_c, of the quantum well as an external potential energy $V_{\rm bare}(z)$, which confines the motion of the electrons in the conduction band. For convenience, we chosen the x-y plane to be parallel and the z direction to be perpendicular to the epitaxial layers of the quantum well, with $z = 0$ at the centre of the quantum well. The electrons are thus confined in the z direction by this potential and their own self-consistent electrostatic field, but free to move in the x-y plane parallel to the epitaxial layers. Within the constant effective-mass approximation, the self-consistent Kohn-Sham eigenfunction may be written as

$$\Psi_J(\mathbf{r}) \equiv \Psi_{k_\parallel,j}(\mathbf{r}) = \frac{1}{2\pi}\exp(\mathbf{k}\cdot\boldsymbol{\rho})\psi_j(z) \tag{1}$$

with eigenenergy

$$E_J \equiv E(\mathbf{k}_\parallel, j) = \varepsilon_j + \frac{1}{2}k_\parallel^2 \tag{2}$$

where $\mathbf{r}$ is a position vector, $\boldsymbol{\rho}$ and z are the projections of $\mathbf{r}$ parallel and normal, respectively, to the epitaxial layers of the quantum well, $\mathbf{k}$ is the wave vector and $\mathbf{k}_\parallel$ is its projection parallel to the interface, ε_j is the eigenenergy and $\psi_j(z)$ is the corresponding eigenfunction of the one-dimentional Schrödinger equation

$$\left[-\frac{1}{2}\frac{d^2}{dz^2} + V(z)\right]\psi_j(z) = \varepsilon_j\psi_j(z). \tag{3}$$

The Green's function for such a one-dimensional system is defined as [12],

$$G^+(z, z', E) = \sum_j \frac{\psi_j^*(z)\psi_j(z')}{E - \varepsilon_j + i\delta} \tag{4}$$

where δ is a small damping parameter used to broaden the poles of the Green's function. It can be shown that the local electron density at point z and energy E is given by

$$\rho(z, E) = -\frac{2}{\pi}\,\mathrm{Im}\; G^+(z, z, E). \tag{5}$$

It can be further shown that

$$\sum_j \delta(E - \varepsilon_j) = -\pi \int dz\; \mathrm{Im}\; G^+(z, z, E) \tag{6}$$

and

$$\psi_j^2(z) = -\frac{1}{\pi}\left[\int_0^{\varepsilon_j^+} dE\; \mathrm{Im}\; G^+(z, z, E) - \int_0^{\varepsilon_j^-} dE\; \mathrm{Im}\; G^+(z, z, E)\right], \tag{7}$$

where $\varepsilon_j^\pm = \varepsilon_j \pm \delta\varepsilon_j$ and $\delta\varepsilon_j$ is the width of the pole at ε_j. Note that $\sum_j \delta(E - \varepsilon_j)$ is the density of states at energy E. The eigenvalues ε_j's are thus given by the locations of the singularities of $\int dz\; \mathrm{Im}\; G^+(z, z, E)$. Therefore, once the Green's function is known, the eigenvalues, eigenfunctions and the local electron density of the system can be obtained from the Green's function.

The Green's function of a quantum well system can be obtained using the invariant embedding method. Consider two plane waves, both originated at z and having energy E, but traveling along the z and $-z$ directions respectively. These plane waves are then scattered by the potential along the z direction. If the resultant amplitude of the scattered plane waves at z is denoted by $D(z, z, E)$, then it can be shown that

$$G(z, z, E) = -\frac{i}{k_z}D(z, z, E) \tag{8}$$

where

$$k_z = \sqrt{2E}. \tag{9}$$

To evaluate $D(z, z, E)$, the propagator, various scattering processes must be considered. Some of the low order scattering processes are shown in Figure 1. Here M_1 and M_2 are reflection coefficients from the potential regions with $(-\infty, z)$ and (z, ∞) respectively. To show these processes, we considered a thin layer of thickness δz in Figure 1. The reflection matrices are obtained by letting $\delta z \longrightarrow 0$. Adding the amplitudes of all the scattered plane waves, we obtain the following expression for the propagator

$$D(z, z, E) = \frac{1 + M_1 + M_2 + M_1M_2}{1 - M_2M_1}\,. \tag{10}$$

The Green's function (8) is therefore given by

$$G(z, z, E) = -\frac{i}{k_z}\frac{1 + M_1 + M_2 + M_1M_2}{1 - M_2M_1}\,. \tag{11}$$

As discussed in reference [8], the reflection matrices M_1 and M_2 are related to the reaction function $R_{k_z}(z)$ by

$$M_1(z) = \frac{ik_zR_{k_z}(z) - 1}{ik_zR_{k_z}(z) + 1}$$

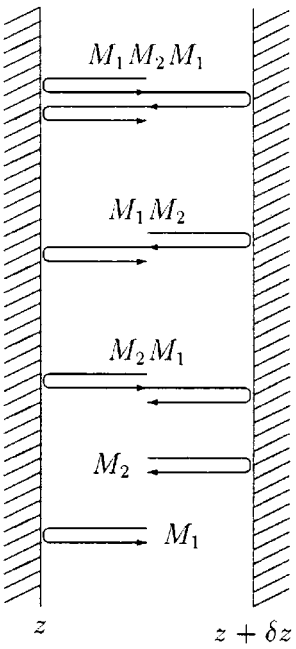

Fig. 1. Some of the low-order scattering processes at plane z from the potential barriers on both sides.

and

$$M_2(z) = \frac{ik_z R_{k_z}(z) + 1}{ik_z R_{k_z}(z) - 1}\,. \tag{12}$$

The reaction function in the above equation is defined by

$$R_{k_z}(z) = \frac{\psi_{k_z}(z)}{\psi'_{k_z}(z)} = \left[\frac{d\ln\psi_{k_z}(z)}{\mathrm{d}z}\right]^{-1} \tag{13}$$

where

$$\psi'_{k_z}(z) = \frac{d\psi_{k_z}(z)}{\mathrm{d}z}\,. \tag{14}$$

The reaction function is expected to be a smoother function of z than $\psi_{k_z}(z)$ itself. Calculation of R_{k_z} has been described in reference [8]. The quantum well region is first divided into thin slices parallel to the well interface such that the potential within each slice can be approximated by a constant. The reaction function is then calculated based on a recurrence relation which relates the reaction function for a given slice to those of other slices and eventually to the boundary conditions.

For a NQW, $V(z)$ approaches a constant for large $|z|$. We can therefore choose a cutoff point z_c such that the potential beyond the cutoff point can be approximated by a constant, *i.e.*

$$V(z) = V(z_\mathrm{c}) \qquad \text{for } |z| \geq z_\mathrm{c}.$$

In the case of a parabolic quantum well (PQW), due to sharp rise in the potential, the electron density decreases rapidly on both sides of the quantum well. Therefore, a cutoff point, z_c, can be chosen such that when $|z| > z_\mathrm{c}$, the potential energy is much larger than the electron energy E and the number of the electrons beyond the cutoff points is negligible. Since the potential energy is so large compared to the electron energy, the electron wave function essentially drops to zero beyond the cutoff points and the actual shape of the potential will not affect the calculated reflection coefficients. We can thus replace the unbounded quadratic potential beyond the cutoff by a simple function such as a constant potential, similar to that for a NQW.

With the above approximation, it can be shown that, for $0 < E < V(z_\mathrm{c})$, the reaction function at the cutoff points are given by

$$R_{k_z}(-z_\mathrm{c}) = \frac{1}{\kappa} \tag{15}$$

and

$$R_{k_z}(z_\mathrm{c}) = -\frac{1}{\kappa} \tag{16}$$

respectively, where

$$\kappa = \sqrt{2[V(z_\mathrm{c}) - E]}. \tag{17}$$

Therefore, for a given quantum well system and a set of boundary conditions, the reflection coefficients at the boundaries can be calculated from equations (15) and (16) and those at an arbitrary point z inside the quantum well can be obtained from the recurrence relation. Equation (11) can then be used to calculate the Green's function, from which the electron density, eigenenergy and eigenfunction can be calculated from equations (5)−(7).

3 Computational details

A GaAs/$Ga_{1-x}Al_xAs$ quantum well can be fabricated with any designed shape for the confining potential by varying the Al concentration from layer to layer in the direction of confinement (z) [15–18]. A PQW is obtained if the average Al concentration varies quadratically in the direction of confinement while a NQW is achieved by changing the Al concentration such that the confining potential is parabolic inside the quantum well but linear outside. According to the Poisson equation, the confining potential $V_\mathrm{bare}(z)$ in a quantum well due to the varying composition along the z direction can be viewed as being produced by a charged slab with a charge density of n^+. In our calculation, such a fictitious positive charge n^+ is used to parametrize the quantum well. The width d of the positively charged region of the slab is defined as the width of a NQW while the approximate width N_s/n^+ of electron distribution is taken to be the width for a PQW. Here N_s is the total number of electrons per unit area and is given by

$$N_\mathrm{s} = \int n(z)\mathrm{d}z. \tag{18}$$

The electron number density $n(z)$ is related to the electron density of states $\rho(z, E)$ given in equation (5) by

$$n(z) = \int_{E \le E_{\rm F}} \rho(z, E) {\rm d}E, \tag{19}$$

where $E_{\rm F}$ is the Fermi energy which can be self-consistently determined by requiring $N_{\rm s}$ to be a predetermined value.

Based on the Kohn-Sham local density approximation [13], the potential acting on an electron can be expressed as

$$V(z) = V_{\rm bare}(z) + V_{\rm e\text{-}e}(z) + V_{\rm xc}(z) \tag{20}$$

where $V_{\rm e\text{-}e}(z)$ is the electrostatic potential due to other electrons and $V_{\rm xc}(z)$ is the exchange-correlation potential. For the given geometry,

$$V_{\rm e\text{-}e}(z) = -4\pi \int_0^z (z - z') n(z') {\rm d}z' \tag{21}$$

and

$$V_{\rm xc}(z) = \left. \frac{\partial (n \epsilon_{\rm xc})}{\partial n} \right|_{n=n(z)} \tag{22}$$

where $\epsilon_{\rm xc}$ is the exchange-correlation energy per particle, which, according to the Wigner interpolation, is given by [14]

$$\epsilon_{\rm xc} = -\frac{0.458}{r_{\rm s}} - \frac{0.44}{r_{\rm s} + 7.8} \tag{23}$$

where

$$r_{\rm s} = r_{\rm s}(z) = \left[\frac{4}{3} \pi n(z) \right]^{-1/3}. \tag{24}$$

Numerical calculation involves two main self-consistent loops. For a given potential, the Fermi energy is first self-consistently determined by requiring the total number of electrons per unit area to be a predetermined value. This self-consistent loop is nested inside another which determines the electron density and potential. Starting with a trial potential and a trial value for the Fermi energy, we first calculate the scattering coefficients using equation (12). Then the Green's function $G(z, z, E)$ is calculated using equation (11) and the local density of states $\rho(z, E)$ is determined using equation (5). Integrating the local density of states $\rho(z, E)$ over energy E gives the electron density $n(z)$ which yields the total number of electrons per unit area. Based on the calculated electron distribution $n(z)$, a potential $V(z)$ is generated from equations (20)-(22), which is used to generate a new set of values for $\rho(z, E)$, $n(E)$ and $E_{\rm F}$. These procedures are repeated until the largest difference between the potential in the present iteration and that in the previous iteration is less than 1% of the maximum value of the potential in the present iteration.

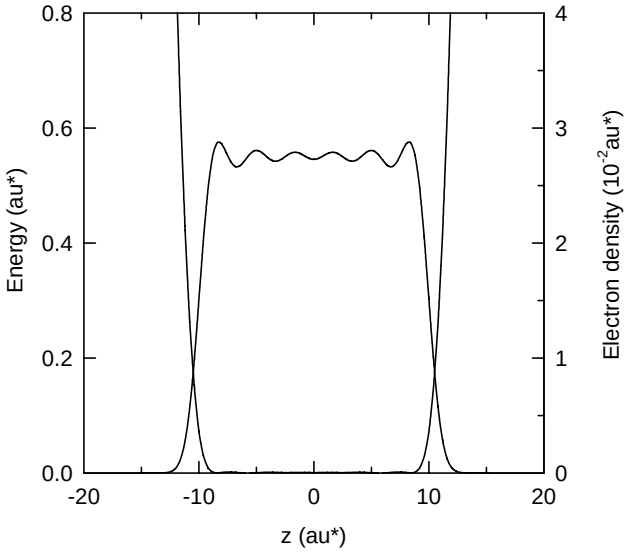

Fig. 2. Self-consistent potential and electron density distribution of a PQW with $d = 20$ au* and $n^+ = 0.0275$ au*.

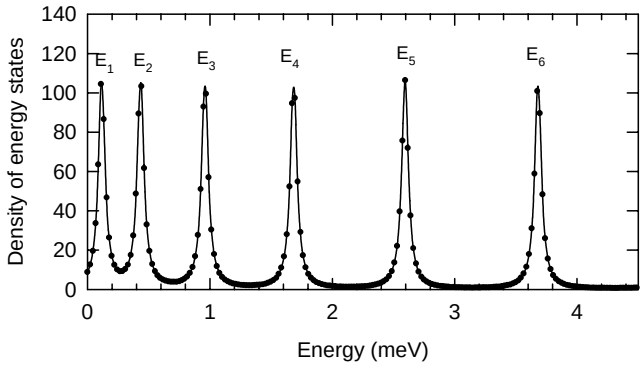

Fig. 3. Density of states of a PQW with $d = 20$ au* and $n^+ = 0.0275$ au*.

The electron density is calculated from equation (19). The integral path along the real axis from 0 to $E_{\rm F}$ is deformed to a semicircle in the upper half of the complex energy plane since the Green's function is analytic in the upper half of the plane. Numerical integration is then carried out using the Gaussian quadrature.

Integrating the Green's function over z yields a function which exhibits a series of sharp peaks. The energy eigenvalues are identified by the positions of these peaks. The squares of the eigenfunctions are calculated using equation (7). In numerical calculation, a small imaginary part ($\delta = 0.03$ au*) is used to broaden the peaks.

One advantage of the present scheme over the solution-following method is the natural integration of the boundary condition into the self-consistent calculation of electronic structure. Since the boundary condition is embedded in the calculation of the reaction function, only changes to the starting point values of R_{k_z} are necessary if different boundary conditions are to be considered.

Furthermore, in the solution-following method, one has to calculate the eigenvalues and eigenfunctions repeatedly in the self-consistent loop which is not only time

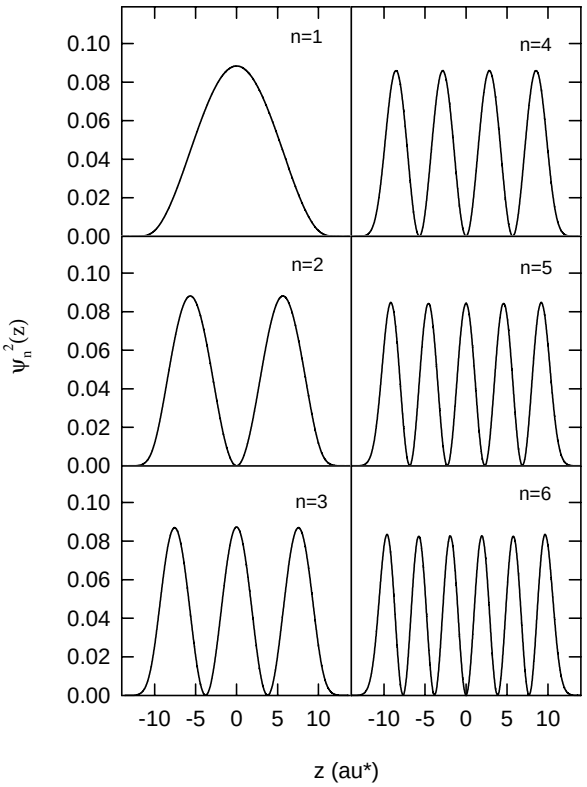

Fig. 4. Eigenfunctions corresponding to the lowest energy subbands of a PQW with $d = 20$ au* and $n^+ = 0.0275$ au*.

consuming, but also less reliable. It is known that a small error in the electron density would induce a relatively large error in the self-consistent potential. The numerical steps in the energy domain therefore must be kept small enough in order to produce acceptable eigenvalues. In the present approach, the electron number density can be obtained simply by integrating the Green's function over a contour in the complex energy plane without calculating the eigenvalues and eigenfunctions. Since the reaction function and thus the Green's function are smooth along the contour in the complex energy plane, only a few mesh points are required in order to achieve an acceptable accuracy in the calculated results. The eigenvalues and eigenfunctions can be calculated, if necessary, from the Green's function after a self-consistent solution has been achieved for the potential and electron density. The present method, therefore, is expected to be a more efficient and reliable scheme for calculation of the electronic structure in such structures.

In the $Ga_{1-x}Al_xAs$ system, the electron effective mass m^* and the dielectric constant ϵ depend weekly on Al concentration [19]. To simplify the calculation, the electron effective mass and the dielectric constant are kept constant and taken to be $0.069m_0$, and 12.9 respectively. Even though the atomic units have been used in the derivations above, the "Hartree Units", au*, in which $e^2/\epsilon = 1$, $m^* = 1$, and $\hbar = 1$, are used in numerical calculation. Note that 1 au* of length is approximately 100 Å while 1 au* of energy is about 11 meV.

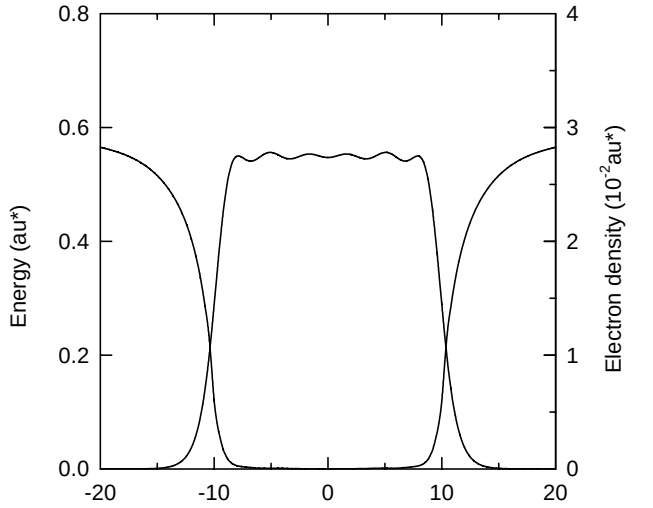

Fig. 5. Self-consistent potential and electron density profiles of a NQW with $d = 20$ au* and $n^+ = 0.0275$ au*.

4 Results and discussion

The present approach based on the invariant embedding method is used to calculate the self-consistent electronic structures in NQW and PQW. The calculated self-consistent potential and electron density distribution for a PQW of width $d = 20$ au* and background density $n^+ = 0.0275$ au* are shown in Figure 2. The electron density inside the quantum well is close to the background density n^+, with a fluctuation of the order of 5% for the major part of the quantum well, and then drops to zero towards the well boundaries. The self-consistent potential is flat at the bottom of the well and rises rapidly on both sides without limit. The results are consistent with those of previous calculations [4,6]. The obtained density of states is presented in Figure 3 as a function of energy. An imaginary part of 0.03 au* has been added to the energy to broaden the peaks. The peak positions give energy eigenvalues below the Fermi energy of the quantum well. The squares of the corresponding eigenfunctions for the different energy eigenvalues calculated from equation (7) are shown in Figure 4.

Calculations are then carried out for the same quantum well but for different charge densities. The calculated energy spacing $(E_F - E_i)$ between the Fermi energy E_F and the bottom of the ith subband E_i are listed in Table 1. Available experimental results and the previously calculated results [20] are also listed in the table for comparison. It can be seen that our calculated subband energy spacing agrees very well with previously calculated results and also in good agreement with experimental results. Therefore it can be concluded that the present approach does produce the electronic structure of a quantum well with excellent accuracy.

We also calculated the electronic structure for a NQW of the same parameters as the PQW considered above, i.e. well width $d = 20$ au* and background density $n^+ = 0.0275$ au*. The obtained potential and electron density profile are shown in Figure 5. It is noted that the PQW

Table 1. The difference between the Fermi energy E_F and the energy at the bottom of the ith subband for parabolic quantum well. n^+ is the positive charge density, n_s is the electron sheet density.

n^+ (10^{15} cm^{-3})	n_s (10^{11} cm^{-2})	Energy (meV)	Exp.[a] (meV)	Calc.[a] (meV)	Present work (meV)
25	2.32	$E_F - E_1$	4.18 ± 0.08	4.18	4.22
		$E_F - E_2$	2.90 ± 0.20	2.99	2.98
		$E_F - E_3$	1.20 ± 0.20	1.16	1.08
6.9	1.37	$E_F - E_1$	2.04 ± 0.07	1.87	1.88
		$E_F - E_2$	1.81 ± 0.07	1.58	1.59
		$E_F - E_3$	1.04 ± 0.07	1.11	1.10
		$E_F - E_4$		0.44	0.43
4.6	0.78	$E_F - E_1$	1.64 ± 0.07	1.37	1.39
		$E_F - E_2$	1.14 ± 0.05	1.01	1.02
		$E_F - E_3$		0.38	0.37

[a] Reference [20].

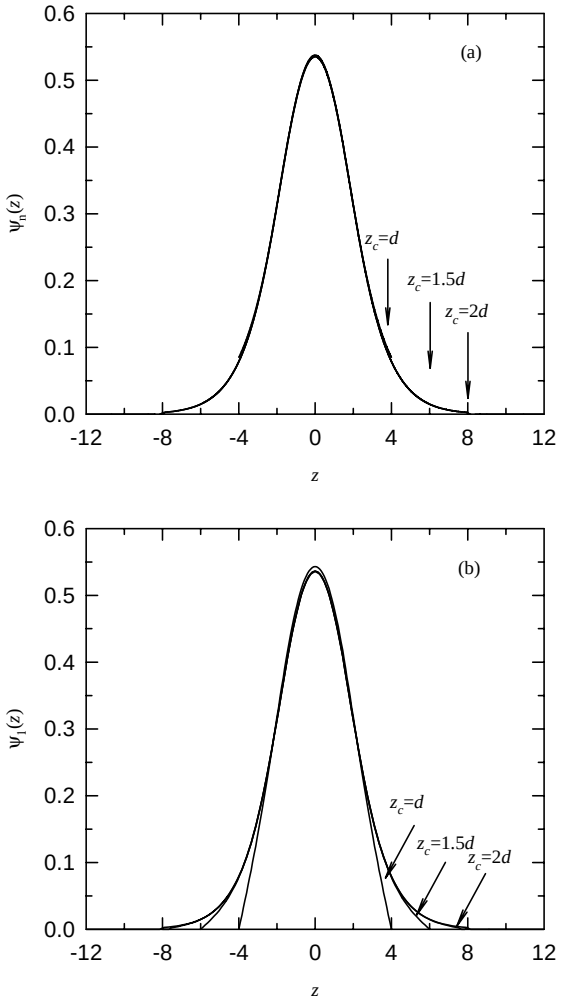

Fig. 6. The wave function of the first subband of a NQW with $d = 4$ au* and $n^+ = 0.0275$ au* calculated using (a) the invariant embedding method and (b) the hard wall boundary condition.

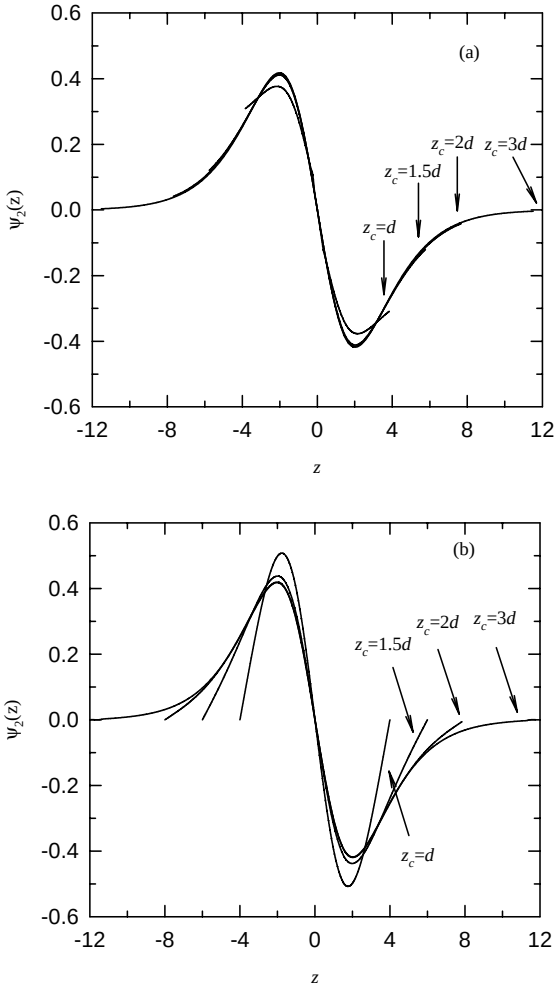

Fig. 7. The wave function of the second subband of a NQW with $d = 4$ au* and $n^+ = 0.0275$ au* calculated using (a) the invariant embedding method and (b) the hard wall boundary condition.

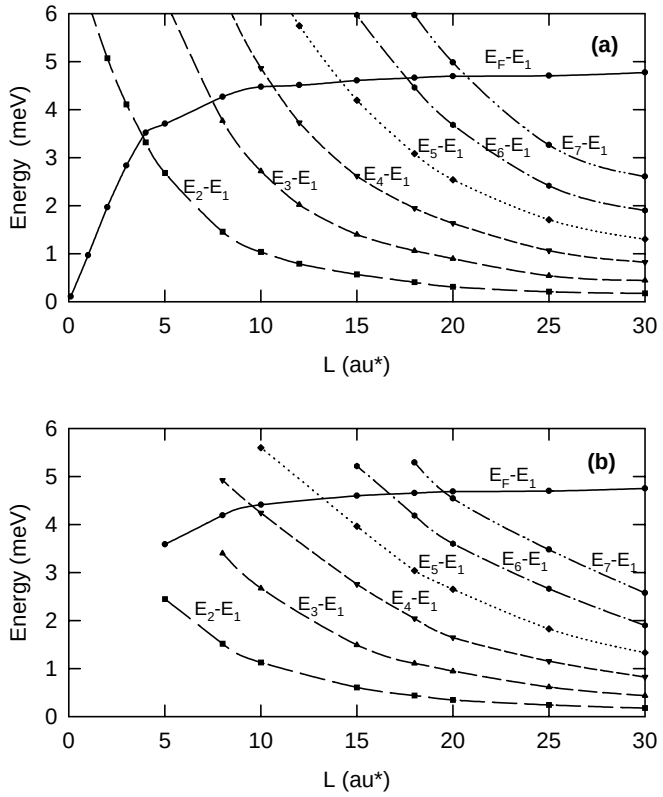

Fig. 8. Different subband energies and Fermi energy of (a) a PQW and (b) a NQW relative to the first subband energy as a function of d. $n^+ = 0.0275$ au* for both structures.

differs systematically from the NQW. First, the variation of the electron density inside the NQW is relatively small compared to that inside the PQW. Second, the electron density profile near the edge of the NQW drops to zero less rapidly than that in the PQW. Third, contrast to the PQW, the self-consistent potential of the NQW approaches a constant value on both sides, which is only slightly larger than the Fermi energy, and the electrons thus penetrate deeply into the barrier regions. This also indicates that the boundary of a NQW is not clearly defined. Ambiguity in choosing the boundary condition may affect the calculated electronic structures, especially in narrow NQWs.

The boundary condition used in the present approach is fundamentally different from that used in the solution-following method. In the latter, two infinite barriers at $z = \pm z_c$ are imposed to make the wave functions vanish at these artificial boundaries. With such "hard wall" boundary condition, electron distribution is confined between the infinite barriers. In a PQW, such an approximation may not cause any significant change to the calculated electron wave function since the potential increases rapidly on both sides of the well. In a NQW, however, the potential approaches a plateau value for large $|z|$ which is only slightly larger than the Fermi energy. Artificially imposed hard walls will change significantly the electron distribution in a NQW. Since the electron distribution near the boundary has a considerable effect on the excitation spectra of a NQW, the shape of edge density profile strongly influences the dynamic response of the system, especially the higher multipole edge plasma modes [21]. In the present work based on the invariant embedding method, a more natural boundary condition is used instead of artificial barriers. A more realistic electron distribution can be obtained. Moreover, the boundary condition is included in the calculation of the reaction function. Therefore, only the starting point values of the reaction function are necessary to be updated should different boundary condition be considered. Various boundary conditions can thus be readily incorporated in the present method. If the calculation region is chosen large enough, the boundary condition may not affect significantly the self-consistent electron structure which only depends on the eigenstates below the Fermi energy level. However, it will significantly change the eigenstates above the plateau value of the self-consistent potential, and hence affects the dynamic response.

Previous theoretical works [4,6,7] have indicated that the boundary condition used in the calculation of electronic structure has a considerable effect on the excitation spectra of NQWs. To further investigate the effects of the boundary, we calculated the electronic structure of a NQW with $d = 4$ au* and $n^+ = 0.0275$ au* using our present approach as well as the solution-following method. In particular, we choose different cutoff points ($z_c = d$, $(3/2)d$, $2d$ and $3d$) in our approach and impose the hard walls also at these locations to see how these choices affect the electronic structure. Two subbands below the Fermi energy are obtained for this NQW. The corresponding wave functions for these two eigenstates are shown in Figures 6 and 7, respectively. In each case, panel (a) shows the results obtained using the present approach while panel (b) displays the profiles calculated using the solution-following method. Clearly for $z_c = d$, the wave functions do not vanish at the boundaries. However, in the solution-following method, the wave function is forced to zero at the boundary. Only when z_c is increased from d to $3d$, the wave functions at the boundaries gradually become to zero. It is also noted that using the present approach, the shapes of the wave functions remain the same when the cutoff z_c is increased from d to $3d$, except for the small deviation when $z_c = d$ in the wave function of the second subband. It clearly demonstrates that the electrons in the well spread to the barrier regions as wide as six times of the well width and the choice of z_c has a significant effect on the shapes of the wave functions in the solution-following method.

Finally we show in Figure 8 the different subband energies and Fermi energy of a PQW and a NQW relative to the first subband energy as a function of d. $n^+ = 0.0275$ au* is used for both the PQW and the NQW. The Fermi energy of the wells rise with the filling up of the first subband. After the first subband is filled, E_F increases slowly as d increases and eventually approaches the bulk value for large d. For wide quantum wells, the subband energy separations $(E_i - E_1)$ of the PQW are nearly the same as those of the NQW. However, for narrow quantum wells

($d < 20$ au*), the subband separations of PQW are larger than those of the NQW.

5 Conclusion

We have presented an approach based on the invariant embedding method for the calculation of electron structure of quantum wells. Applications to both NQW and PQW have demonstrated that the method can be used to calculate self-consistent electronic structure and potential of quantum wells. Numerical results obtained for these structures agree very well with those of previous theoretical works and experimental data. The present method can also provide information about the energy eigenvalue and eigenfunction of each individual state. It is expected to be more efficient and numerically more stable than the solution-following method. Furthermore the present method can be extended to the calculation of excitation spectra of quantum well structures, which will be discussed elsewhere.

References

1. N.D. Lang, W. Kohn, Phys. Rev. B **1**, 4555 (1970).
2. F. Stern, S. Darma, Phys. Rev. B **30**, 840 (1984).
3. A.J. Rimberg, R.M. Westervelt, Phys. Rev. B **40**, 3970 (1989).
4. J.F. Dobson, Phys. Rev. B **46**, 10163 (1992).
5. C. Kittle, *Quantum Theory of Solids* (John Wiley and Sons, 1963).
6. J.F. Dobson, Aust. J. Phys. **46**, 391 (1993).
7. W.L. Schaich, J.F. Dobson, Phys. Rev. B **49**, 14700 (1994).
8. H.C. Poon, P.T. Howe, Mod. Phys. Lett. **6**, 459 (1992).
9. D. Serest, *Atom-Molecule Collision Theory*, edited by R.B. Bernstein (Plenum, 1979); J.C. Light, R.B. Walker, J. Chem. Phys. **65**, 4272 (1976).
10. T.C. Zhao, H.C. Poon, S.Y. Tong, Phys. Rev. B **38**, 1172 (1988).
11. M.G. Burt, J. Phys.-Cond. Matter **4**, 6651 (1992).
12. E.N. Economou, *Green's function in quantum physics* (Spring-Verlag, 1979).
13. W. Kohn, L.J. Sham, Phys. Rev. A **10**, 1133 (1995).
14. D. Mahan, *Many Particle Physics* (Plenum, New York, 1989).
15. M. Sundaram, A.C. Gossard, J.H. English, R.H. Westervelt, Superlatt. Microstruct. **4**, 683 (1988).
16. M. Shayegan, T. Sajoto, M. Santos, C. Silvestre, Appl. Phys. Lett. **53**, 791 (1988).
17. S. Giugni, T.L. Tansley, J. Vac. Sci. Technol. B **9**, 2805 (1991).
18. W.Q. Chen, S.M. Wang, T.G. Anderson, J. Thordson, Phys. Rev. B **48**, 14264 (1993).
19. S. Adachi, *Properties of Aluminium Gallium Arsenide* (Inspec. London, 1993).
20. P.F. Hopkins, A.J. Rimberg, E.G. Gwinn, R.M. Westervelt, M. Sundaram, A.C. Gossard, Appl. Phys. Lett. **57**, 2823 (1990).
21. Q. Guo, Y.P. Feng, H.C. Poon, C.K. Ong, J. Phys.-Cond. Matter **8**, 9037 (1996).